A Compressed N×N Multi-Pixel Imaging and Cross Phase-Detection AF with N×1RGrB + 1×NGb Hetero Multi-Pixel Image Sensors

Koichi Fukuda[1,2]

[1] ICB R&D Center 1, Canon Inc.
30-2, Shimomaruko 3-chome, Ohta-ku, Tokyo, Japan 146-8501
Tel: +81-3-3758-2111, E-mail address: fukuda.koichi@mail.canon

[2] Graduate School of Engineering, Tohoku University
6-6-11-811, Aza-Aoba, Aramaki, Aoba-ku, Sendai, Miyagi, Japan 980-8579
Tel: +81-22-795-4833, Email address: fukuda.koichi.p3@dc.tohoku.ac.jp

ABSTRACT

We propose a 25M-pixel full-frame horizontal 2×1RGrB + vertical 1×2Gb hetero dual-pixel image sensor and a new effective algorithm to restore high-quality 2×2 quad-pixel image data. This proposed camera architecture can make the number of pixels and the amount of data 50% reduced. Moreover, we apply this architecture to a horizontal 5×1RGrB + vertical 1×5Gb hetero penta-pixel image sensor as a 5×5 pentacosa-pixel light field camera; this technology can reduce 80% of the data.

INTRODUCTION

Sensor-based phase-detection autofocus (PDAF) with a dual-pixel image sensor [1-6] is one of the most important functions to perform fast and accurate AF in digital interchangeable lens cameras (DILCs).

Fig.1 shows the optical relationships between photodiodes A through D, pupils A through D, and viewpoint images A through D in a 2×2 quad-pixel camera [7-8].

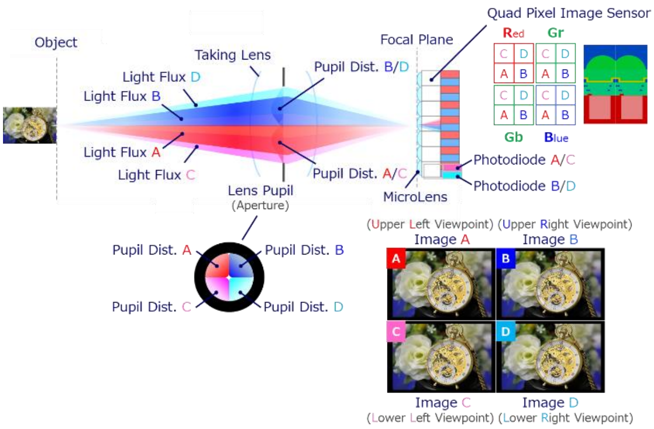

Fig.1 The optical system of a 2×2 quad-pixel camera. Light rays with incident angles as from pupils A through D of a taking lens are received by photodiodes A through D, respectively.

The horizontal 2×1 dual-pixel image sensor in Fig.2 (a) can detect as PDAF only vertical lines using the horizontal parallax and not horizontal lines. On the other hand, the 2×2 quad-pixel image sensor in Fig.2 (b) can detect as PDAF both vertical and horizontal lines. However, the 2×2 quad-pixel image sensor needs twice the number of pixels, and the reading speed of the sensor will be slower by half [5]. As a result, it makes rolling shutter distortion larger or vertical PDAF performance lower when shooting high-speed moving objects.

To resolve the above tradeoff, we propose a 25M-pixel full-frame horizontal 2×1RGrB + vertical 1×2Gb hetero dual-pixel image sensor in Fig.2 (c) and a new effective algorithm to create 2×2 quad-pixel image data. This proposed camera architecture can make the number of pixels and the amount of data 50% reduced.

Moreover, we apply this architecture to a 5×1RGrB+1×5Gb hetero penta-pixel image sensor in Fig.15 (b) and reduce 80% pixels of a light field camera.

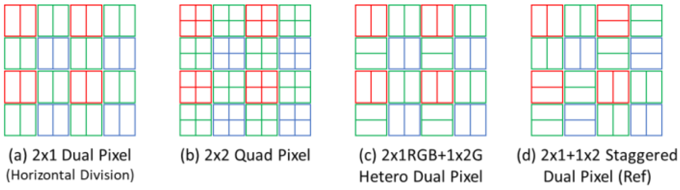

Fig.2 Layout diagrams of pixel array patterns.

QUAD-PIXEL CAMERA WITH HETARO DUAL-PIXEL SENSOR

To verify the principle, we made prototyping a 4.14μm 50M-pixel full-frame 2×2 quad-pixel image sensor. Then, we compared the proposed 25M-pixel hetero dual-pixel pattern (c) and the other 50M-pixel quad-pixel pattern (b) and 25M-pixel staggered dual-pixel pattern (d) shown in Fig.2.

Fig.3 (a) shows the diagonal cross-section of the prototype 2×2 quad-pixel with a 4-peak microlens and the light intensity distribution in the pixels using Finite-Difference Time-Domain (FDTD) simulation of an electromagnetic wave having a wavelength λ of 540nm. An ordinary pixel in Fig.3 (b) has each microlens formed on each photodiode. In contrast, the prototyped pixels in Fig.3 (a) have one microlens synthesized from 4 eccentric sub-microlenses formed on 2×2 photodiodes. In Fig.4, the experimental/simulation data of the pupil intensity distributions of the prototyped pixels HA(=A+C), HB (=B+D), and I (=A+B+C+D) are shown by solid/dotted red, blue, and green lines, respectively.

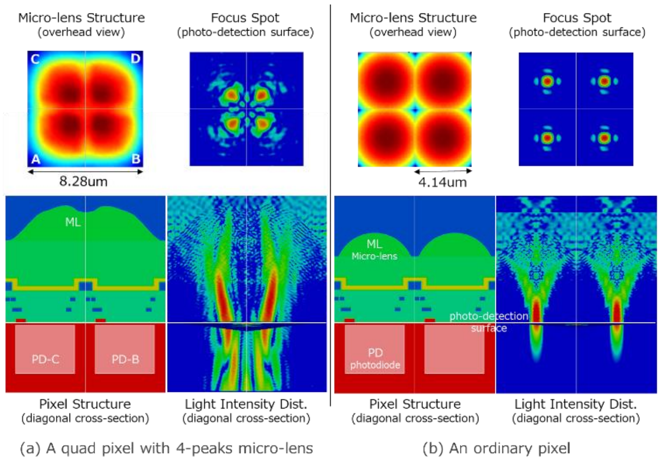

Fig.3 The diagonal cross-section of the prototype 2×2 quad-pixel with a 4-peak microlens and the light intensity distridution.

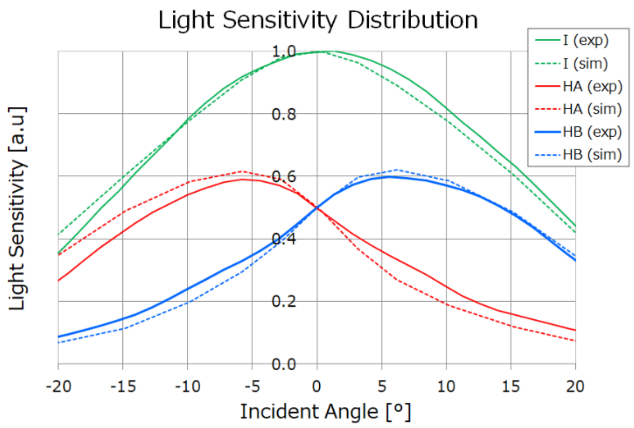

Fig.4 The pupil intensity distribution of the prototype 2×2 quad-pixel image sensor.

QUAD-PIXEL RESTORATION ALGORITHM

There are two fundamental reasons why the proposed algorithm can restore high-resolution 2×2 quad-viewpoint images from the compressed hetero dual-pixel data in Fig.2 (c).

The first is the higher symmetry of the hetero dual-pixel than other patterns, such as the staggered dual-pixel in Fig.2 (d) in terms of horizontal and vertical division G pixels determining the resolution. On the hetero dual-pixel, for each vertical division Gb pixel, horizontal division Gr pixels are arranged at all four diagonal nearest neighbors, and vice versa.

The second is that the standard image I (=A+B+C+D) can be used as reference data at all positions regardless of horizontal or vertical division pixels.

In detail, first, we restore the left/right viewpoint image HA(=A+C) /HB(=B+D) at position (ix,iy+1) of each Gb pixel in Fig.5. The numerator is the sum of the left/right viewpoint images HA/HB(ix±1,iy+1±1) at four diagonal neighbors of Gr pixels. The denominator is the sum of the images I(ix±1,iy+1±1) of Gr pixels. The left/right viewpoint image HA/HB (ix,iy+1) of the Gb pixel in Fig.5 equals the image I(ix,iy+1) multiplied by the ratio of the numerator divided by the denominator.

Second, we create the upper/lower viewpoint image VA(=A+B) /VB(=C+D) at (ix+1,iy) of each Gr, similarly in Fig.6.

Third, we restore the upper/lower viewpoint image VA/VB at (ix,iy) of each R pixel in Fig.7. The numerator is the sum of the upper/lower viewpoint images VA/VB at four nearest neighbors (ix±1,iy) and (ix,iy±1) of G pixels. The denominator is the sum of the images I(ix±1,iy) and I(ix,iy±1) of G pixels. The upper/lower viewpoint image VA/VB(ix,iy) of the R pixel in Fig.7 equals the image I(ix,iy) of the R pixel multiplied by the ratio of the numerator divided by the denominator.

Fourth, we create the upper/lower viewpoint image VA/VB (ix+1,iy+1) of each B pixel, similarly in Fig.8.

Finally, we approximate the 2×2 quad-viewpoint images A= min[HA(=A+C),VA(=A+B)], B= min[HB(=B+D),VA(=A+B)], C= min[HA(=A+C),VB(=C+D)], D= min[HB(=B+D),VB(=C+D)].

Fig.10 shows 2×2 quad-viewpoint images A through D restored by the proposed algorithm from the hetero dual-pixel data, and Fig.11 (b) shows the partially enlarged image A of Fig.10. Even though the hetero dual-pixel data is 50% reduced, these restored images can be as high resolution as the original quad-viewpoint images of the quad-pixel in Fig.9 and Fig.11 (a). In contrast, the reference image A of the staggered dual-pixel in Fig.11 (d) is lower resolution than others.

Fig.13 shows the defocus map detected horizontally and vertically by the hetero dual-pixel sensor as cross PDAF. The defocus map of the hetero cross PDAF is also as high performance as the original one of the quad-pixel sensor in Fig.12.

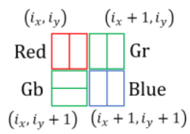

$$I(i_x,i_y) = A(i_x,i_y) + B(i_x,i_y) + C(i_x,i_y) + D(i_x,i_y).$$

$$HA(i_x,i_y) = A(i_x,i_y) + C(i_x,i_y),\quad HB(i_x,i_y) = B(i_x,i_y) + D(i_x,i_y).$$

$$VA(i_x,i_y) = A(i_x,i_y) + B(i_x,i_y),\quad VB(i_x,i_y) = C(i_x,i_y) + D(i_x,i_y).$$

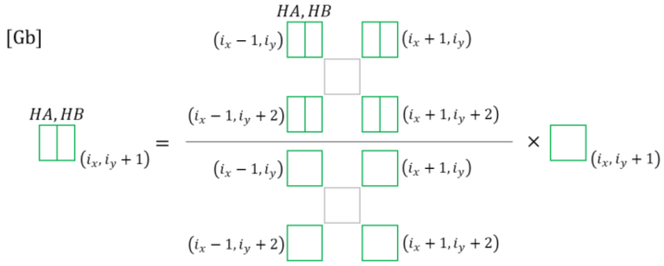

[Gb]

$$HA(i_x,i_y+1) = \frac{HA(i_x-1,i_y)+HA(i_x+1,i_y)+HA(i_x-1,i_y+2)+HA(i_x+1,i_y+2)}{I(i_x-1,i_y)+I(i_x+1,i_y)+I(i_x-1,i_y+2)+I(i_x+1,i_y+2)} \times I(i_x,i_y+1),$$

$$HB(i_x,i_y+1) = \frac{HB(i_x-1,i_y)+HB(i_x+1,i_y)+HB(i_x-1,i_y+2)+HB(i_x+1,i_y+2)}{I(i_x-1,i_y)+I(i_x+1,i_y)+I(i_x-1,i_y+2)+I(i_x+1,i_y+2)} \times I(i_x,i_y+1).$$

Fig.5 The proposed algorithm restoring the left/right viewpoint data HA/HB of Gb pixels.

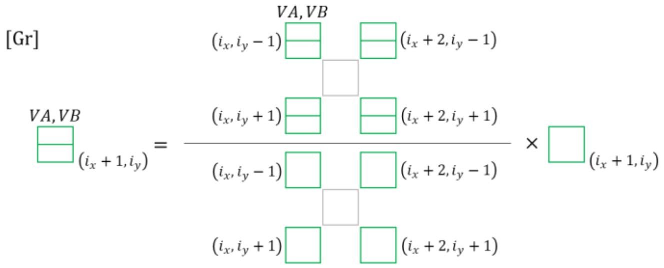

[Gr]

$$VA(i_x+1,i_y) = \frac{VA(i_x,i_y-1)+VA(i_x+2,i_y-1)+VA(i_x,i_y+1)+VA(i_x+2,i_y+1)}{I(i_x,i_y-1)+I(i_x+2,i_y-1)+I(i_x,i_y+1)+I(i_x+2,i_y+1)} \times I(i_x+1,i_y),$$

$$VB(i_x+1,i_y) = \frac{VB(i_x,i_y-1)+VB(i_x+2,i_y-1)+VB(i_x,i_y+1)+VB(i_x+2,i_y+1)}{I(i_x,i_y-1)+I(i_x+2,i_y-1)+I(i_x,i_y+1)+I(i_x+2,i_y+1)} \times I(i_x+1,i_y).$$

Fig.6 The proposed algorithm restoring the upper/lower viewpoint data VA/VB of Gr pixels.

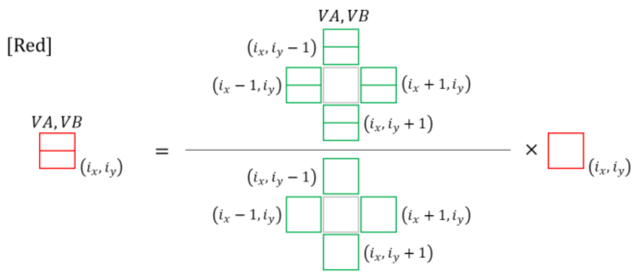

[Red]

$$VA(i_x,i_y) = \frac{VA(i_x,i_y-1)+VA(i_x-1,i_y)+VA(i_x+1,i_y)+VA(i_x,i_y+1)}{I(i_x,i_y-1)+I(i_x-1,i_y)+I(i_x+1,i_y)+I(i_x,i_y+1)} \times I(i_x,i_y),$$

$$VB(i_x,i_y) = \frac{VB(i_x,i_y-1)+VB(i_x-1,i_y)+VB(i_x+1,i_y)+VB(i_x,i_y+1)}{I(i_x,i_y-1)+I(i_x-1,i_y)+I(i_x+1,i_y)+I(i_x,i_y+1)} \times I(i_x,i_y).$$

Fig.7 The proposed algorithm restoring the upper/lower viewpoint data VA/VB of R pixels.

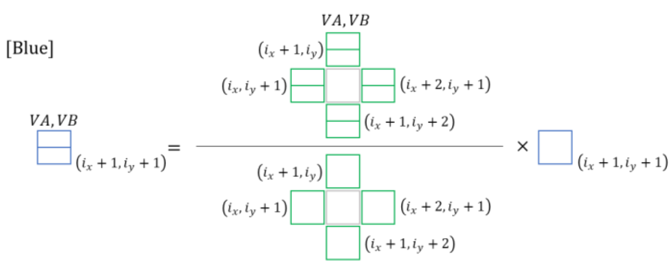

[Blue]

$$VA(i_x+1,i_y+1) = \frac{VA(i_x+1,i_y)+VA(i_x,i_y+1)+VA(i_x+2,i_y+1)+VA(i_x+1,i_y+2)}{I(i_x+1,i_y)+I(i_x,i_y+1)+I(i_x+2,i_y+1)+I(i_x+1,i_y+2)} \times I(i_x+1,i_y+1),$$

$$VB(i_x+1,i_y+1) = \frac{VB(i_x+1,i_y)+VB(i_x,i_y+1)+VB(i_x+2,i_y+1)+VB(i_x+1,i_y+2)}{I(i_x+1,i_y)+I(i_x,i_y+1)+I(i_x+2,i_y+1)+I(i_x+1,i_y+2)} \times I(i_x+1,i_y+1).$$

Fig.8 The proposed algorithm restoring the upper/lower viewpoint data VA/VB of B pixels.

2x2-Viewpoint Images (2x2 Quad Pixel)

Fig.9 12.5M 2×2 quad-viewpoint images of the 2×2 quad-pixel image sensor.

2x2-Viewpoint Images (2x1RGB+1x2G Hetero Dual Pixel)

Fig.10 12.5M 2×2 quad-viewpoint images of the 2×1RGB+1×2G hetero dual-pixel image sensor.

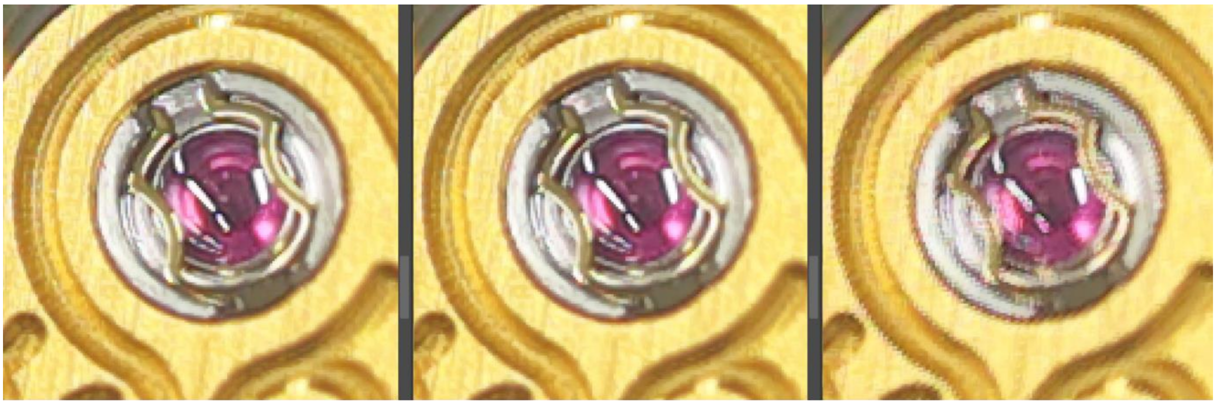

(a) 2×2 Quad-Pixel (b) 2×1RGB+1×2G Hetero Dual-Pixel (c) 2×1+1×2 Staggered Dual-Pixel (Ref)

Fig.11 A resolution comparison diagram

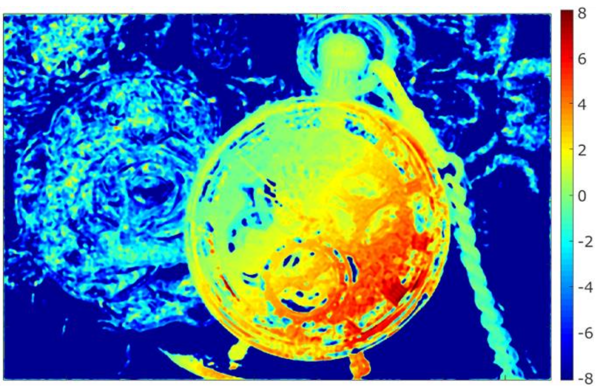

Defocus Map (2x2 Quad Pixel)

Fig.12 A defocus map example of the 2×2 quad-pixel image sensor.

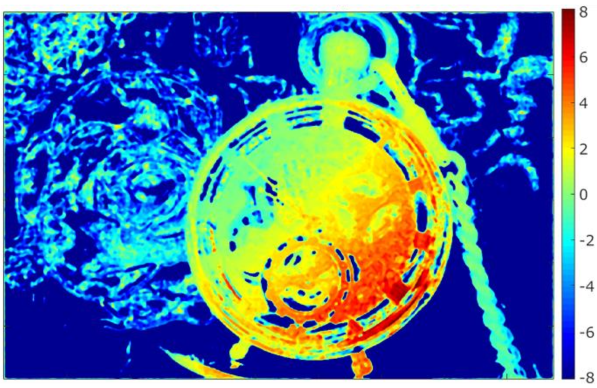

Defocus Map (2x1RGB+1x2G Hetero Dual Pixel)

Fig.13 A defocus map example of the 2×1RGB+1×2G hetero dual-pixel image sensor.

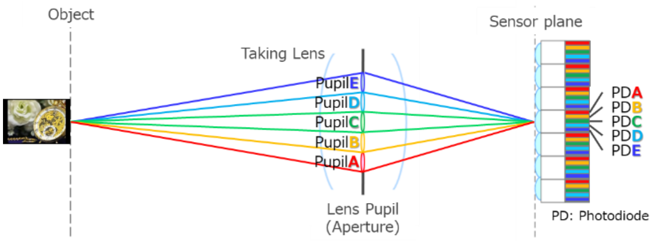

Fig.14 The optical system of a 5×5 pentacosa-pixel camera.

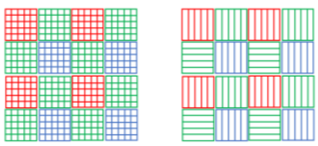

(a) 5x5 Pentacosa Pixel (b) 5x1RGB+1x5G Hetero Penta Pixel

Fig.15 Layout diagrams of pixel array patterns.

Fig.16 5×5 pentacosa-viewpoint images of the 5×1RGB+1×5G hetero penta-pixel image sensor.

PENTACOSA-PIXEL CAMERA WITH HETERO PENTA-PIXEL SENSOR

A light field camera needs more divided pixels and viewpoint images than a sensor-based PDAF camera to realize a post-shooting function or computational photographic functions, such as refocus [9]. Therefore, the reduction of the data is more critical.

Fig.14 and Fig.15 (a) show the optical system of a 5×5 pentacosa-pixel camera as a light field camera. The more divided pixels, the more effectively the developed new architecture can reduce the data. Hence, we apply the proposed architecture to a 5×5 pentacosa-pixel light field camera with a horizontal 5×1RGrB + vertical 1×5Gb hetero penta-pixel image sensor in Fig.15 (b), similarly.

To verify the principle, we made prototyping a 5.16μm approximately 9.4M-pixel 19.35mm×12.9mm 5×5 pentacosa-pixel image sensor. Then, we compared the proposed 1.88M-pixel 5×1RGrB+1×5Gb hetero penta-pixel data reduced by 80% in Fig.15 (b) and the original 9.4M-pixel 5×5 pentacosa-pixel data in Fig.15 (a).

Fig.16 shows 5×5 pentacosa-viewpoint images from upper-left H1V1 to lower-right H5V5 restored by the proposed algorithm from the 5×1RGrB+1×5Gb hetero penta-pixel data, and Fig.18 shows the enlarged upper-left viewpoint image H1V1 of Fig.16. On the other hand, Fig.17 shows the enlarged upper-left viewpoint image H1V1 of the original 5×5 pentacosa-pixel image sensor.

Even though the 5×1RGrB+1×5Gb hetero penta-pixel data is 80% reduced, the restored image H1V1 in Fig.18 can be as high resolution as the original image H1V1 in Fig.17.

Moreover, because of the signal addition of five pixels, the restored upper-left viewpoint image H1V1 in Fig.18 is much smoother than the original upper-left viewpoint image H1V1 in Fig.17.

CONCLUSION AND DISCUSSION

We developed the 25M-pixel full-frame horizontal 2×1 RGrB + vertical 1×2Gb hetero dual-pixel image sensor and the new effective algorithm restoring high-resolution 2×2 quad-pixel images; this technology reduced 50% of the data.

Moreover, we applied this architecture to the horizontal 5×1RGrB + vertical 1×5Gb hetero penta-pixel image sensor as a 5×5 pentacosa-pixel light field camera; this reduced 80% of the data.

To generalize and summarize, we proposed compressed horizontal N×1RGrB + vertical 1×NGb hetero multi-pixel image sensors and the effective algorithm to restore the N×N multi-pixel image data. This camera architecture can reduce the number of pixels to 1/N in multi-pixel cameras.

In future work, we consider that it is necessary to develop the backside-illuminated (BSI) stacked CMOS image sensor based on the proposed camera architecture for realizing high-performance horizontally and vertically cross PDAF in high-speed continuous shooting. It is also necessary to research practical computational photographic functions with this technology.

REFERENCES

[1] N. L. Stauffer, US Patent 4,410,804, 1983.

[2] K. Fukuda, “Phase-difference detection AF with a dual pixel image sensor”, 40th Optical Symposium Proceedings, pp.91-94, 2015, [in Japanese].

[3] M. Kobayashi, M. Johnson, Y. Wada, H. Tsuboi, T. Ono, H. Takada, K.Togo, T. Kishi, H. Takahashi, T. Ichikawa, and S. Inoue, “A Low Noise and High Sensitivity Image Sensor with Imaging and Phase-Difference Detection AF in All Pixels”, 2015 Int. Image Sensor Workshop, p.24, 2015.

[4] S. Yokogawa, I. Hirota, I. Ohdaira, M. Matsumura, A. Morimitsu, H.Takahashi, T. Yamazaki, H. Oyaizu, Y. Incesu, M. Atif, and Y. Nitta, “A 4M pixel full-PDAF CMOS image sensor with 1.58μm 2X1 On-Chip Micro-Split-Lens technology”, 2015 Int. Image Sensor Workshop, p.28, 2015.

[5] K. Fukuda, US Patent 9,794,468 B2, 2017.

[6] E. S. Shim, K. Lee, J. Pyo, et.al, “All-Directional Dual Pixel Auto Focus Technology in CMOS Image Sensors”, 2021 Symposium on VLSI Circuits, 2021.

[7] K. Fukuda, US Patent 8,773,549 B2, 2014.

[8] T. Okawa, S. Ooki, H. Yamajo, M. Kawada, M. Tachi, K. Goi, T. Yamasaki, H. Iwashita, M. Nakamizo, T. Ogasahara, Y. Kitano, K. Tatani, “A 1/2inch 48M All PDAF CMOS Image Sensor Using 0.8μm Quad Bayer Coding 2×2OCL with 1.0lux Minimum AF Illuminance Level”, 2019 IEDM, pp.16.3.1-16.3.4, 2019.

[9] R. Ng, M. Levoy, M. Brédif, G. Duval, M. Horowitz, P. Hanrahan, "Light Field Photography with a Hand-Held Plenoptic Camera", Stanford Tech Report CTSR 2005-02, April, 2005.

Fig.17 An upper-left-viewpoint image of the 5x5 pentcosa-pixel image sensor.

Fig.18 An upper-left-viewpoint image of the 5x1RGB+1x5G hetero penta-pixel image sensor.